

## Gravity Wave Turbulence in Wave Tanks: Space and Time Statistics

Sergei Lukaschuk,<sup>1,\*</sup> Sergey Nazarenko,<sup>2</sup> Stuart McLelland,<sup>3</sup> and Petr Denissenko<sup>4</sup>

<sup>1</sup>Department of Engineering, Hull University, Hull, HU6 7RX, United Kingdom

<sup>2</sup>Mathematics Institute, Warwick University, Coventry, CV4 7AL, United Kingdom

<sup>3</sup>Department of Geography, Hull University, Hull, HU6 7RX, United Kingdom

<sup>4</sup>School of Engineering, Warwick University, Coventry, CV4 7AL, United Kingdom

(Received 19 November 2008; published 22 July 2009)

We present the first simultaneous space-time measurements for gravity wave turbulence in a large laboratory flume. We found that the slopes of  $k$  and  $\omega$  wave spectra depend on wave intensity. This cannot be explained by any existing theory considering wave turbulence as the result of either breaking events or weakly nonlinear wave interactions. Instead, we show that random waves and breaking or coherent structures appear to coexist: The former show themselves in a quasi-Gaussian core of the probability density function and in the low-order structure functions, and the latter in the probability density function tails and the high-order structure functions.

DOI: 10.1103/PhysRevLett.103.044501

PACS numbers: 47.35.Bb, 47.35.Jk

Recently, there has been significant progress in understanding the gravity water wave turbulence (WT) theoretically [1–7], with the help of numerical modeling [5,8–10], field observations [11], and laboratory experiments [12–14]. In our recent experiments in a large 2D flume [14], we reported observations of WT with nonuniversal frequency spectra whose slope changed from  $-6$  to  $-4$  as the wave intensity increases. We explained this slope variation by suppression of resonant wave interactions due to finite size effects at lower amplitudes and by breaking waves at higher amplitudes.

However, there still remains an uncertainty about important physical processes since the same frequency spectrum could arise from completely different theories. This uncertainty could be resolved by measuring the  $k$  spectra which are different for these cases or, even better, by simultaneous measurement and juxtaposition of the  $\omega$  and the  $k$  spectra. Furthermore, random waves and coherent structures or breaks show different signatures in the high-order statistics of the wave elevations. Breaking waves, in turn, may be of different kinds, ranging from the progressive-wave breaks with a limiting angle of  $120^\circ$  typical for the open seas to vertical jet ejections typical for the breaking of standing waves or waves reflected by walls [15,16]. In laboratory flumes, it is not *a priori* clear which kind will dominate, because a large nonlinearity leading to breaking at the same time leads to wave decorrelations and respective departure from the standing-wave structure of the linear eigenmodes. To find which type of breaking dominates, one can look for the wave break signatures in the high-order statistics. With these motivations in mind, we report here the first results on the statistics of gravity wave turbulence obtained from simultaneous  $t$  and  $x$  measurements in the laboratory flume. We used the data collected to analyze the  $\omega$  and the  $k$  spectra as well as the higher-order structure functions in the  $t$  and the  $x$  domains.

The experiments were conducted in the tank described in Ref. [14] with an area of  $12 \times 6$  m and a depth of 0.9 m. A wave maker generated a superposition of two equal amplitude waves with frequencies  $f_1 = 0.993$  Hz and  $f_2 = 1.14$  Hz. The angle between wave vectors  $\mathbf{k}_1$  and  $\mathbf{k}_2$  was  $9^\circ$ , and  $\mathbf{k}_1$  was perpendicular to the plane of the wave maker. At sufficiently large wave amplitudes, a chaotic wave field is formed in the middle area of the flume due to multiple wave reflections and nonlinear interactions.

We used capacitance probes to measure the wave elevation as a function of time  $\eta(t)$ . To obtain variations of the wave elevation in space, we implemented an imaging technique, similar to Ref. [17], with a thin vertical laser light sheet illuminating the fluorescent surface layer of water from below. The size of the imaged area was  $1151 \times 478$  mm in the horizontal and vertical directions, respectively, with a resolution of 0.9 mm. Typically, we collected 1200 images during a 20-minute time interval simultaneously with the continuous capacitance probe measurement. This time interval defines an upper time scale for statistical averages. The water surface boundary  $\eta(x)$  was detected from the images using standard MATLAB binarization and edge detection procedures. Images where the boundary was not a single-valued function of  $x$  or when it had significant jumps [ $|\delta\eta(x)/\delta x| > 4$ ] were excluded (less than 3% of the total number).

All of the measurements described here were undertaken with fixed excitation parameters and a stationary wave field. To characterize the wave field intensity, we use a nonlinearity parameter which is defined as the mean wave slope at the energy containing the scale  $\gamma = k_m A$ , where  $k_m$  is the wave number corresponding to the maximum of the energy spectrum  $|\eta_\omega|^2$  and  $A$  is the rms of  $\eta(t)$ . To minimize the effects of the finite size of the flume on the resonant wave interactions [4,5], we limited our observations to sufficiently strong wave fields with  $0.1 < \gamma < 0.25$ .

Most statistical wave theories predict universal energy spectra  $E_k \propto k^{-\mu}$  and  $E_\omega \propto \omega^{-\nu}$  with  $\mu, \nu = \text{const}$ . There are three different predictions for  $\mu$  and  $\nu$  (leaving aside the case of very weak waves [4,5]). In the weak turbulence theory,  $\mu = 5/2$ ,  $\nu = 4$  [Zakharov-Filonenko (ZF) slopes [3,18]]. Based on a dimensional argument, Phillips predicted  $\nu = 5$  [7]. Kuznetsov [19] considered 1D breaks propagating with a preserved shape and velocity  $V$ , which corresponds to a Doppler-type dispersion law  $\omega = kV$  and the spectral slopes  $\mu = \nu = 4$  (Ku slopes). Kuznetsov also pointed out that in this setup the Phillips  $\nu = 5$  would correspond to 0D (pointlike) breaks and, respectively,  $\mu = 3$  (Ph slopes). A more complicated fractal distribution of 1D breaks was put forward in Ref. [20] which resulted in the same slopes as Ku.

Our experimental spectra have relatively wide scaling ranges in  $\omega$  and  $k$ ; see, e.g., Fig. 1 for a  $k$  spectrum and Ref. [14] for the  $\omega$  spectra. The slopes  $\mu$  of the energy spectra in the  $k$  domain as a function of the wave field intensity ( $I = |\eta_\omega|^2$ ,  $\omega = 2\pi f$ , and  $f = 3$  Hz) are shown in Fig. 2(a). A similar amplitude dependence for the indices  $\nu$  of the  $\omega$  spectra was already presented in our previous work [14]. Both  $\nu$  and  $\mu$  gradually decrease when the wave intensity (nonlinearity)  $\gamma$  increases.

Figure 2(b) shows the simultaneously measured  $k$  and  $\omega$  slopes. As we see, the experimental points deviate significantly from the linear dispersion relation  $\omega = \sqrt{gk}$ , which indicates that the wave nonlinearity is not weak. We also show the points corresponding to the Ph, ZF, and Ku slopes. While both the Ph and the Ku points are rather far from the experimental data, the ZF point could be obtained by extrapolation to the higher wave amplitudes. This result is rather surprising, because one would expect the ZF theory to work better for weaker waves. However, the finite flume size effects are more important for weaker waves, which explains why there is a significant deviation from the ZF spectrum at smaller wave amplitudes. With the possibility to measure the  $k$  spectra, we can now resolve an uncertainty between the ZF and the Ku predictions

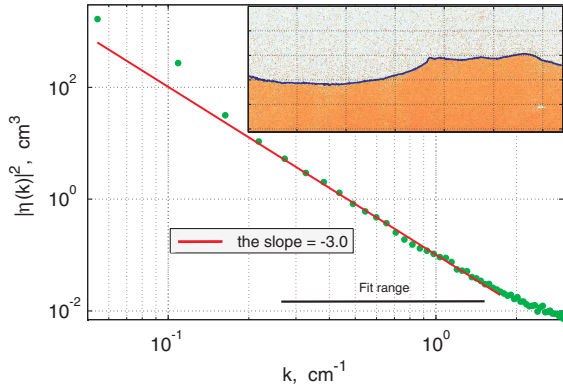


FIG. 1 (color online). A spectrum in the  $k$  domain. The inset shows an image with the detected boundary on the air-water interface.

(both of which give the same slope in the  $\omega$  domain). From Fig. 2(b), one can conclude that both theories are not confirmed exactly by our experiment, with the ZF predictions somewhat closer to the observations. The Ku-type breaks seem quite rare and do not contribute to the spectra [and the second-order structure function (SF)]; nevertheless, they may leave their imprints on the scalings of the high-order SF, as will be seen below. The dependence of the spectral exponents on the wave intensity is likely to be due to both the finite size effects and the increased number of breaks or structures when the amplitude increases. Visual observations show a variety of break types: Some occur on the ridges of running waves and some as localized vertical splashes. The prevalence of a particular break morphology is likely to be affected by the finite flume size via the interference of waves reflected from the walls.

In order to distinguish between particular kinds of coherent structures and incoherent random waves (which sometimes have the same spectra), let us consider the higher-order correlators. By analogy with hydrodynamic turbulence, our object for the high-order statistics will be not the wave elevation itself but its space and time increments of different orders. The latter are defined as  $\delta_l^{(1)} = \eta(\mathbf{x} + l) - \eta(\mathbf{x})$  and  $\delta_l^{(2)} = \eta(\mathbf{x} + l) - 2\eta(\mathbf{x}) + \eta(\mathbf{x} - l)$ , etc., for spatial and as  $\delta_\tau^{(1)} = \eta(t + \tau) - \eta(t)$  and  $\delta_\tau^{(2)} = \eta(t + \tau) - 2\eta(t) + \eta(t - \tau)$ , etc., for temporal variables. In  $\delta_l^{(i)}$ , all  $\eta$ 's are taken at the same  $t$  and in  $\delta_\tau^{(i)}$  at the same  $x$ .

The moments of the increments, known as the *structure functions*, are defined as  $S_l^{(j)}(p) = \langle (\delta_l^{(j)})^p \rangle$  and  $S_\tau^{(j)}(p) = \langle (\delta_\tau^{(j)})^p \rangle$  for the space and the time domains, respectively, where the angle brackets denote averaging over  $x$  or  $t$ . For a stationary random process characterized by a power-law spectrum, the structure functions will also vary as power laws  $S_l^{(j)}(p) \sim l^{\xi(p)}$  and  $S_\tau^{(j)}(p) \sim \tau^{\zeta(p)}$  in the limits of small  $l$  and  $\tau$ , respectively. The scaling exponents  $\xi(p)$  and  $\zeta(p)$  contain information about the turbulence intermittency and participating random-phased and coherent components. If we assume that our wave field is composed of modes with random phases, then the height increments

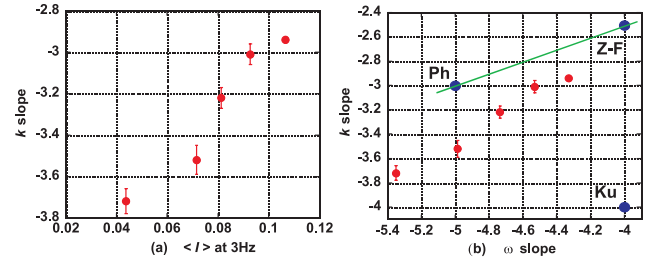


FIG. 2 (color online). Slopes of the wave spectra. (a) The  $k$  slope as a function of wave intensity. (b) The  $k$  slope vs the  $\omega$  slope. The linear dispersion relation  $\omega = \sqrt{gk}$  is shown by the solid line.

should follow the Gaussian statistics. For this case we can calculate (see for details [21])  $S_l^{(j)}(p) \sim l^{p(\mu-1)/2}$  if  $\mu < 2j + 1$ ; otherwise,  $S_l^{(j)}(p) \sim l^{pj}$  because the field is  $j$  times differentiable. Similarly, in the time domain we have for the random-phased field  $S_\tau^{(j)}(p) \sim \tau^{p(\nu-1)/2}$  if  $\nu < 2j + 1$ ; otherwise,  $S_\tau^{(j)}(p) \sim \tau^{pj}$ .

The SFs for a class of singularities with the profile  $\eta(x) = \text{const} - A|x|^a$  with  $0 < a \leq 1$  and  $A > 0$  were calculated in Ref. [21] for singularities of different (possibly fractal) dimensions  $D$ :  $0 \leq D < 2$  (e.g., 0 for Ph and 1 for Ku). Parameter  $a > 0$  describes the singularity strength; e.g., for  $a < 1$  the breaks are sharper than the Ku-type  $\Lambda$ -shaped ridges at  $a = 1$ . Such singular coherent structures give  $S_l^{(j)}(p) \sim l^{pj} + l^{2-D+ap}$ . The first term in this expression is a contribution of the smooth humps, and the second one is due to the coherent structures. In the limit  $l \rightarrow 0$ , the term with the smallest power will be dominant. Thus, the structures of Ph or Ku type, i.e., with  $a = 1$ , would not be seen for the first-order increments, and we would have to consider  $j \geq 2$ . However, one should keep in mind that the finite range of excited scales makes determination of the scalings less precise for higher  $j$  because of the larger number of SF points to be placed in this finite range. Therefore, it is better to consider the lowest  $j$  for which the scalings induced by the coherent structures can be extracted ( $j = 2$  in case of the Ph and Ku).

Now suppose that the wave field is bifractal and consists of two components: random-phased modes and singular coherent structures. Avoiding the choices of  $j$  for which the field is  $j$  times differentiable, we have in this case  $S_l^{(j)}(p) \sim l^{p(\mu-1)/2} + l^{2-D+ap}$ . If  $a < (\mu - 1)/2$ , we expect to see the scaling associated with the incoherent random-phased component at low  $p$ 's (first term on the right-hand side) and the singular coherent structure scaling at high  $p$ 's (second term on the right-hand side).

Similarly, one can consider the SFs of the time increments. Assuming, following Kuznetsov, that the coherent structures could be thought of as passing the wire probes with constant velocity, we should obtain the time-domain scalings to be identical to the space-domain scalings, i.e.,  $S_\tau^{(j)}(p) \sim \tau^{2-D+ap}$ . For the incoherent component,  $S_\tau^{(j)}(p) \sim \tau^{p(\nu-1)/2}$ . Assuming again that incoherent waves and the singular structures are present simultaneously, we have  $S_\tau^{(j)}(p) \sim \tau^{p(\nu-1)/2} + \tau^{2-D+ap}$ . As before, the order  $j$  is chosen in such a way that the field associated with the incoherent wave component is not  $j$  times differentiable in time. For example, for spectra with  $3 < \nu < 5$  (e.g., for the ZF spectrum) one should use  $j \geq 2$ , and for  $5 < \nu < 7$  one should use  $j \geq 3$ , etc.

To present results on the probability density functions (PDFs) and the SFs, we select the experimental run with spectra  $E_k \sim k^{-3.02}$  and  $E_\omega \sim \omega^{-4.53}$ . Because for each of these spectra both  $k$  and  $\omega$  slopes are steeper than  $-3$  but shallower than  $-5$ , we choose to work with the second-

order increments,  $j = 2$ . Experimental PDFs of the height increments in space and time are shown in Fig. 3(a) and 3(b), respectively. For the space increments, one can see clearly deviations from Gaussianity at the (fat) PDF tails which are related to intermittency and indicate the presence of the coherent structures. For the time increments, the deviations from Gaussianity are much less pronounced, which could be due to the slow propagation speed of the coherent structures leading to their more infrequent occurrence in the  $t$  domain in comparison with the  $x$  domain. Both the  $t$ - and the  $x$ -domain PDFs are asymmetric (with the negative increments dominant) which results from breaks occurring at wave crests rather than troughs.

In our data on the SFs, both  $S_\tau^{(2)}(p)$  as a function of  $\tau$  and  $S_l^{(2)}(p)$  as a function of  $l$  exhibit clear power-law scalings in the range of scales corresponding to the gravity waves for all  $p$  at least up to 8; see Fig. 3(c) [due to the lack of space, we present only  $S_l^{(2)}(p)$ ]. The SF exponents for the time and space domains are shown in Fig. 4. Straight lines in these graphs represent the ZF scaling (solid red line), scaling of waves with the spectrum as measured in the experiment (dashed green line), and the fit of the high- $p$  behavior with a scaling corresponding to singular coherent structures (dashed-dotted blue line). For the time domain, the scaling at low  $p$  is close to the ZF scaling; this is surprisingly more consistent than with the scaling calculated from the actual measured spectrum. For an infinite scaling range, the  $p = 2$  point must, of course, lie exactly on the value corresponding to the spectrum ( $\nu - 1$ ) irrespective of the presence or absence of the phase correlations. Thus we attribute the observed discrepancy to the finite size of the scaling range. Furthermore, the fit of the high  $p$  dependence indicates the presence of singular coherent structures with  $D = 1$  and  $a = 1.05$  that is very close to the Ku's  $D = 1$  and  $a = 1$ .

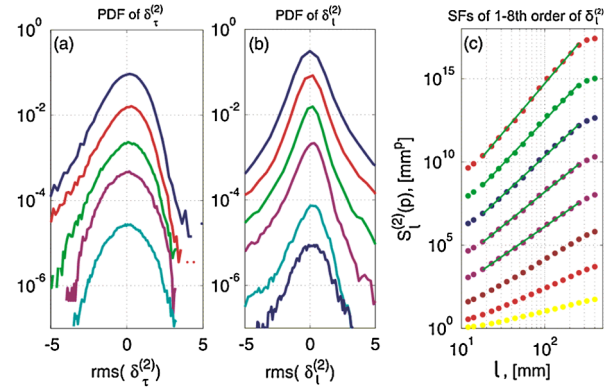


FIG. 3 (color online). PDFs of the second-order differences: (a) in the  $t$  domain,  $\tau = 30, 60, 130, 290$ , and  $580$  ms (from the top down); (b) in the  $x$  domain,  $l = 54, 11, 25, 62, 149$ , and  $360$  mm (from the top down); (c) SFs of  $\delta_t^{(2)}$  for  $p = 1, \dots, 8$ .

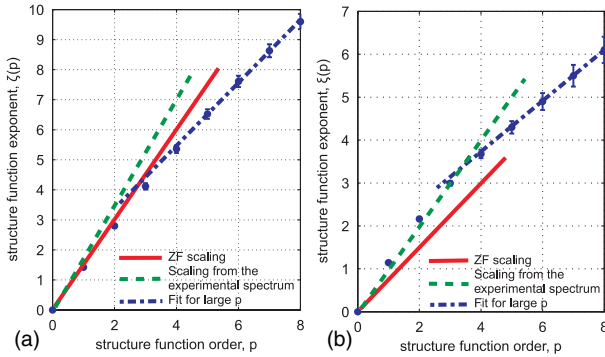


FIG. 4 (color online). SF scaling exponents: (a)  $\zeta(p)$  in the  $t$  domain and (b)  $\xi(p)$  in the  $k$  domain.

For the space domain, at low  $p$  there is an agreement with the scaling of the random-phased waves having the actual measured spectrum and less agreement with the random-phased waves having the ZF spectrum. This is not surprising since the scaling range in  $k$  is greater than in  $\omega$ , and therefore there is a better agreement between the spectrum and the SF exponent for  $p = 2$ . More importantly, we see again the dominance of the random-phased waves in the low-order SFs and the dominance of coherent breaks in the high-order SFs. The fit at high  $p$ 's gives for the dimension and the singularity parameter of the breaks  $D = 1.3$  and  $a = 1/2$ , respectively. We see that the breaks appear to be more singular and “spiky” than the Ku-type breaks ( $a = 1$ ). Visually, we observed numerous occurrences of these kinds of spiky wave breaks, which are propagating very slowly and producing vertical splashes. These kinds of structures should be probable in isotropic wave fields due to the collision of counterpropagating waves, which in our flume appear due to wave reflections from the walls. The slow propagation speed of such breaks means that they cross through the capacitance probe infrequently even if there is a large number of them in the  $x$  domain (i.e., more than the Ku-type breaks). This could explain why the Ku breaks show up in the SF scalings in the  $t$  domain, whereas more singular spiky structures are seen in the  $x$  domain.

In summary, our experimental data show that the spectral exponents, in both  $\omega$  and  $k$ , depend on the amplitude of the forcing. None of the existing theories that rely on either the presence of random-phased weakly nonlinear waves or the dominance of coherent wave crests of a particular type can fully explain these results. Instead, there is an indication that the gravity wave field consists of coexisting and interacting random and coherent wave components, as it was speculated before from open-sea radar measurements [22]. The random waves are captured by the PDF cores and the low-order SFs, whereas the coherent wave crests leave their imprints on the PDF tails and on the high-order SFs. The wave crests themselves consist of structures of differ-

ent shapes: numerous nonpropagating spikes or splashes (which show in the  $x$ -domain SFs) and propagating Ku-type breaks (seen in the  $t$ -domain SFs). We hope that our technique based on SF scalings can be useful in future for analyzing the open-sea data, as well as to the future WT theory describing the dynamics and mutual interactions of these coexisting random-phased and coherent wave components.

This work was partially done during the EPSRC sponsored Warwick Turbulence Symposium program. The authors are grateful to the Hull Environmental Research Institute for a financial support and B. Murphy for his help with the flume experiments.

\*Also at The Institute of Automation and Electrometry, SBRAS, Novosibirsk, Russia.

S.Lukaschuk@hull.ac.uk

- [1] A. C. Newell and V. E. Zakharov, Phys. Lett. A **372**, 4230 (2008).
- [2] V. E. Zakharov, V. S. L'vov, and G. Falkovich, *Kolmogorov Spectra of Turbulence* (Springer-Verlag, Berlin, 1992).
- [3] V. E. Zakharov and N. N. Filonenko, J. Appl. Mech. Tech. Phys. **4**, 506 (1967).
- [4] S. V. Nazarenko, J. Stat. Mech. (2006) L02002.
- [5] Y. Lvov, S. Nazarenko, and B. Pokorni, Physica (Amsterdam) **218D**, 24 (2006).
- [6] V. E. Zakharov, A. O. Korotkevich, A. N. Pushkarev, and A. I. Dyachenko, JETP Lett. **82**, 487 (2005).
- [7] O. M. Phillips, J. Fluid Mech. **4**, 426 (1958).
- [8] M. Onorato *et al.*, Phys. Rev. Lett. **89**, 144501 (2002).
- [9] A. I. Dyachenko, A. O. Korotkevich, and V. E. Zakharov, Phys. Rev. Lett. **92**, 134501 (2004).
- [10] S. Y. Annenkov and V. I. Shrira, J. Fluid Mech. **449**, 341 (2001).
- [11] P. A. Hwang *et al.*, J. Phys. Oceanogr. **30**, 2753 (2000).
- [12] E. Falcon, C. Laroche, and S. Fauve, Phys. Rev. Lett. **98**, 094503 (2007).
- [13] Y. Toba, J. Oceanogr. Soc. Jpn. **29**, 209 (1973).
- [14] P. Denissenko, S. Lukaschuk, and S. Nazarenko, Phys. Rev. Lett. **99**, 014501 (2007).
- [15] M. J. Cooker and D. H. Peregrine, in *Coastal Engineering, Proceedings of the ICCE Conference, Delft, Holland* (ASCE, Reston, VA, 1990), Vol. 1, pp. 164–176.
- [16] M. S. Longuet-Higgins, J. Fluid Mech. **248**, 449 (1993).
- [17] M. A. Mukto, M. A. Atmane, and M. R. Loewen, Exp. Fluids **42**, 131 (2007).
- [18] S. A. Kitaigorodskii, Bull. Acad. Sci. USSR, Geophys. Ser. **1**, 105 (1962).
- [19] E. A. Kuznetsov, JETP Lett. **80**, 83 (2004).
- [20] S. E. Belcher and J. C. Vassilicos, J. Fluid Mech. **342**, 377 (1997).
- [21] S. Nazarenko, S. Lukaschuk, S. McLelland, and P. Denissenko, arXiv:0811.2579.
- [22] V. Kudryavtsev *et al.*, J. Geophys. Res. **108**, 8054 (2003).